Nuclear Instruments and Methods 172 (1980) 281–285
©North-Holland Publishing Company

DIFFRACTION EFFICIENCIES OF HOLOGRAPHIC TRANSMISSION GRATINGS IN THE REGION 80–1300 eV

J.P. DELVAILLE, H.W. SCHNOPPER
Smithsonian Astrophysical Observatory, Cambridge, Mass. 02138 USA

E. KÄLLNE
Department of Physics, University of Virginia, Charlottesville, Virginia 22901, USA

I. LINDAU, R. TATCHYN, R.A. GUTCHECK *
Stanford Synchrotron Radiation Laboratory, Stanford, Ca. 94305 USA

R.Z. BACHRACH,
Xerox Palo Alto Research Center, Palo Alto, Ca. 94304 USA

J.H. DIJKSTRA
The Astronomical Institute, Space Research Laboratory, Utrecht, The Netherlands

Experimental measurements of diffraction efficiencies for holographic transmission gratings have been performed. The transmitted intensity distribution is characterized by an overall efficiency of about 10% into first order and a strong resonance enhancement, up to 20% efficiency, around the region of anomalous dispersion. The intensity distribution is well described by a grating model which predicts the overall efficiency, as well as the detailed behavior of the grating around the regions of anomalous dispersion. The model can be used to predict the efficiencies for an arbitrary grating material and thickness, and thus aid in the determination of grating structure for a specific experimental application.

1. Introduction

We have already shown the promising features of self-supporting holographic transmission gratings in the soft X-ray region [1,2]. Also, during the last few years the transmission gratings have been investigated by other groups [3,4]. The possibilities of using transmission gratings combined with grazing incidence optics as applied to systems for applications in space are very appealing, as well as for monochromators at synchrotron radiation facilities and as tools in plasma diagnostics. Our efforts during the last two years have been directed towards obtaining enough data for different types of transmission gratings over a wide wavelength region so as to verify and extend our model for these systems.

In addition to new data obtained at SSRL we present a sample of the calibration data for a complete set of 160 gratings mounted into the X-ray telescope on the HEAO-2 satellite.

* Present address: SRI International, Menlo Park, Ca. 94025 USA.

2. Grating structure

The continuing development of the grating structure and fabrication procedures have led to several improvements and created new possibilities as to the possible variety of grating material and structure that will be available in the near future. For example, the rather extreme requirements imposed by the application in space have led to a development of a grating with a regular support structure that has greatly reduced any scattering compared with the random support structure used earlier [5]. This has facilitated the construction of stronger grating structures. Furthermore, the difficulty of producing thicker (>4000 Å) gratings seems to be a temporary obstacle as we now are planning to use a well defined thin grating structure as a lithographic mask. This has opened up new possibilities for the designing of the grating system as we will point out in this paper. The grating structures we have used so far have had line spacing of 500 and 1000 l mm^{-1}, a mark–space ratio of 0.40–0.60 and thickness of 700–1800 Å. In fig. 1 are displayed some typical grating structures as photographed by electron microscope using different magnifications.

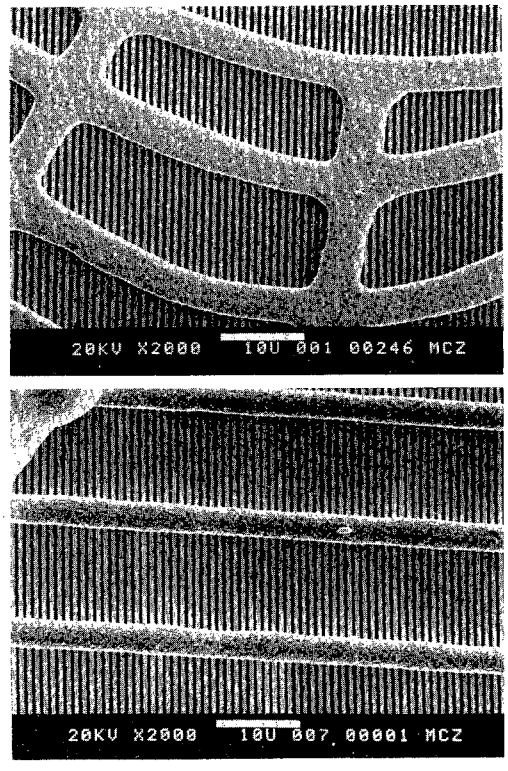

Fig. 1. Electron microscope picture of two transmission gratings with 1000 l mm^{-1}.

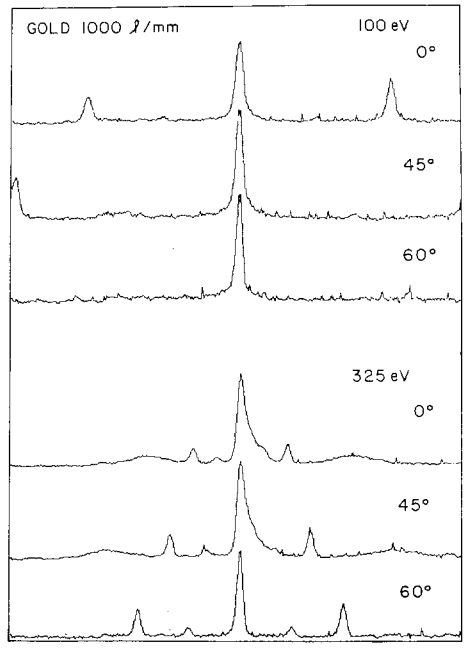

Fig. 2. Experimental data for the transmitted intensity distribution through a 870 Å thick gold grating with a line density 1000 l mm^{-1} at two different incoming photon energies and three different angles of incidence.

3. Diffraction efficiency measurements

We have already described the experimental procedure we have developed using the soft X-ray (4°) beam line at the Stanford Synchrotron Radiation Laboratory [1,2]. The transmission grating tests have proven useful in the measurement of the diffraction efficiencies of the transmission gratings as well as in the analysis of the composition of the synchrotron radiation beam from the grazing incidence monochromator ("The Grasshopper") [6]. In fig. 2 we show the experimental data for our last measurements at two photon energies, 100 and 325 eV. We have extended the wavelength region from previous experiments and investigated the behavior of the grating upon rotation around an axis parallel to the wires. There are several interesting features which can be seen from the figure. First, the spectrum at 100 eV is free from any scattered light and upon rotation of the grating the first order moves out beyond the edges of the figure. At higher energies, there are contributions from the second order diffraction from the "Grasshopper" as well as scattered light in a broad distribution on each side of the zero order. The increased dispersion of the transmission grating upon rotation results in clearly resolved first order diffraction maxima of the incoming photon energy as well as the second order from the "Grasshopper". The width of the zero order peak is limited by the size of the focal spot (the size of the detector slit was 0.5 mm). The scattered light from the "Grasshopper" introduces an uncertainty for the efficiency measurements owing to the concommitant zero order contribution which is difficult to estimate. This is especially true at higher energies as the scattered light intensity increases and the first order diffraction maximum sits on a dispersed broad background distribution. However, it has been possible to correct for most of the scattered light at intermediate energies because the scattered light beam is slightly offset from the monochromatic beam. At high energies we can iterate the model to correct for the now unresolvable scattered light zero-order peak.

We have tested thin gratings (~1000 Å) with regular and random support structures over a region of 80–1300 eV using continuous synchrotron radiation with the transmission gratings perpendicular to the photon beam as well as at varying angles. The

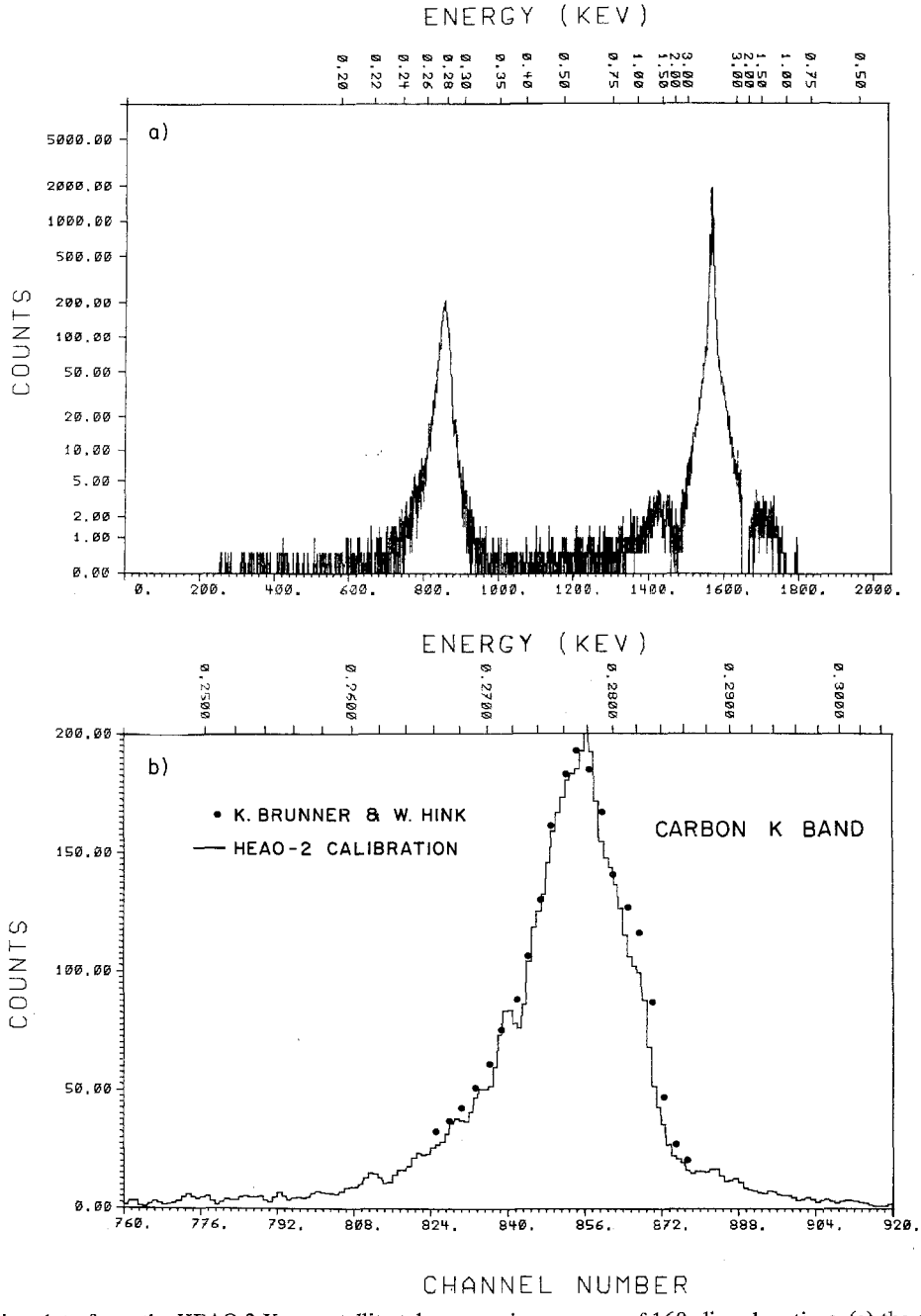

Fig. 3. Calibration data from the HEAO-2 X-ray satellite telescope using an array of 160 aligned gratings. (a) the carbon K in zero and first order, (b) carbon K in detail (———) HEAO-2 data, (· · · · ·) ref. [7].

diffracted light pattern as a function of photon energy is characterized by an overall efficiency of about ten percent in each first order beam with a strong resonant enhancement at the region of anomalous dispersion (at the minimum in absorption coefficient preceding the Au N edge). The position and intensity of the resonance is strongly dependent on the grating properties, and thus constitute a sensitive probe for a modelling of the grating behavior.

The gratings to be used in the HEAO-2 satellite were tested prior to launch in a facility at Marshall Space Flight Center in Huntsville, Alabama. The test

station consisted of a demountable X-ray tube, a vacuum pipe approximately 1000 feet long and the telescope including the gratings. An example of the many calibration spectra recorded with gold gratings of 1000 l mm^{-1} is shown in fig. 3. The recorded Carbon K spectrum shows that the gratings work reasonably well as a spectrometer. The resolution, while adequate for space requirements, is limited however, as the gratings were not used in a configuration corrected for coma. As a result the energy resolution $\Delta E/E$ is limited to 1/100. However, the spectral features from the Carbon K spectrum are clearly resolved as seen from the comparison with the spectrum recorded at higher resolution [7].

4. Modelling of the gratings

From the electron micrographs, we measure thickness and mark–space ratio and determine the shape of the wires. At normal incidence the diffracted intensity distribution is modelled as described in our earlier paper [1]. The model neglects multiple scattering as well as any kind of edge effects (e.g., small angle scattering) in the grating wires. The model contains two parameters: grating thickness, and mark–space ratio. A least squares fit finds the optimum values for these in several different ways for a single grating as well as for the 160 gratings in the telescopic mount. The fit procedure is done both at a fixed energy for all the diffraction orders as well as for one order over the whole energy region. As already mentioned, the resonance structure at ~130 eV is a very sensitive measure for the model predictions, and we have been able to fit all the grating data with this model. Also, rotation of the grating may be included in the model as shown in Appendix 1. The line density is an additional parameter in this case. An example of the relative efficiency into first order for one grating at three angular settings is shown in fig. 4. The intensity distribution from the rotated grating has also been modelled in detail elsewhere [8].

In the model, we have used the optical constants from Hagemann et al. [9] which are the only available data for this energy region. These constants are measured in the lower energy region by absorption measurements while the higher energy region has been studied with reflectivity measurements and adjusted to the absorption data to achieve an overlap. There are few data points available at higher energies which make it difficult to predict the grating behavior

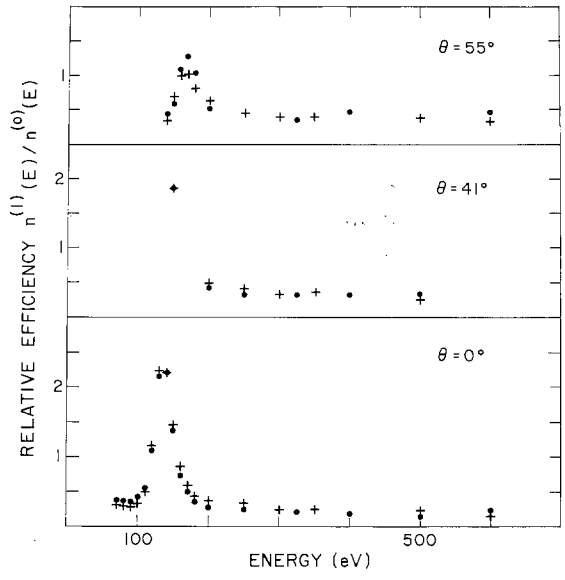

Fig. 4. Relative efficiency data into first order for a 1000 l mm^{-1} gold grating at three different angles. The crosses are the experimental values and the dots show the model predictions using a thickness of 868 Å and a mark–space ratio of 0.53.

at the higher energies. Therefore, we are currently developing grating experiments in order to measure the optical constants using well-defined grating structures [10].

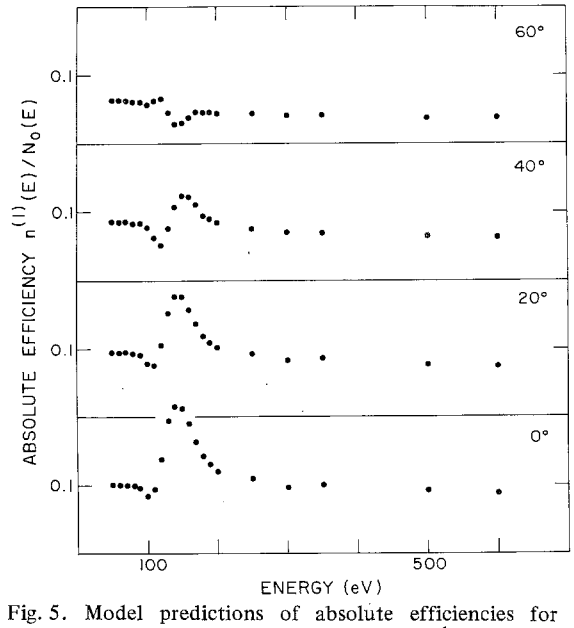

Fig. 5. Model predictions of absolute efficiencies for a 1000 Å thick gold grating of 1000 l mm^{-1}, mark–space ratio 0.5 at four different incidence angles.

Figure 5 shows the absolute efficiency predicted by the model for various angles of incidence. The support structure of a real grating obscures part of the light and we have measured actual obscuration factors ranging from 45–60%. Therefore the absolute efficiencies given in fig. 5 must be multiplied by an obscuration factor of the order of one-half. It must be emphasized, however, that owing to the lack of optical constants, the model cannot be reliably extended beyond 300 eV. Moreover, around 2 keV where the Au M absorption edge starts, there will be another resonance enhancement in the efficiency curve. It is of interest here to note that Bräuninger et al. [4] quote a value for the efficiency as high as 40% at the lower resonances around 7 Å.

5. Conclusions

The model behavior of a transmission grating upon rotation shows that this system can be used as the basic structure for a monochromator. For a high flux and moderate resolution system, the rotating transmission grating together with a focusing grazing incidence mirror can readily select a given wavelength from a continuous synchrotron radiation spectrum. It is also feasible to imagine a focusing transmission grating structure [11]. The analysing transmission grating could either be used over a wide wavelength region with ten percent efficiency if the grating is thick enough, or in a limited wavelength region taking advantage of the enhanced efficiency due to anomalous dispersion. Furthermore, the two diffracted first order beams could either be used separately or again focused together for a higher throughput. Thus, with this detailed knowledge of the grating behavior, it is now possible to construct a multipurpose monochromator in the soft X-ray region.

Appendix 1

Bräuninger et al. [4] have given an expression for the diffraction efficiencies of X-rays normally incident on transmission gratings with trapezoidal wire shapes. We have adapted their equations to describe the X-ray diffraction efficiencies of transmission gratings with rectangular wire cross sections rotated through an angle θ about an axis paralleled to the wires. Their eqs. (1) and (2) respectively, become:

$$\frac{n^{(m)}(K)}{N_0(K)} = \left| \sum_{l=0}^{3} f_{l,l+1}^{(m)}(k) \right|^2 (d \cos\theta)^{-2}, \qquad \text{(A1)}$$

Table 1 [a]

l	X_l	Z_l	C_l
0	0	0	0
1	$a \cos\theta - b \sin\theta$	0	$1/(\sin\theta \cos\theta)$
2	$a \cos\theta$	$b/\cos\theta$	0
3	$d \cos\theta - b \sin\theta$	$b/\cos\theta$	$-1/(\sin\theta \cos\theta)$
4	$d \cos\theta$	–	–

[a] $d - a$ and b are the width and thickness respectively.

and

$$f_{l,l+1}^{(m)}(k) = \frac{1}{kR} \exp[-\mathrm{i} \cos^{-1}(\beta C_l/R) + \mathrm{i}k(Z_l - C_l X_l)(\delta + \mathrm{i}\beta)] \times [\![\exp\{\mathrm{i}x_{l+1}[kC_l(\delta + \mathrm{i}\beta) + \phi]\} - \exp\{\mathrm{i}x_l[kC_l(\delta + \mathrm{i}\beta) + \phi]\}]\!]. \qquad \text{(A2)}$$

Where m = order; β = imaginary part of the refractive index; $1 - \delta$ = real part of the refractive index; d = grating periodicity; $\phi = 2\pi m/(d \cos\theta)$; k = photon energy E in units of $\hbar c$; $kR = [(C_l k\beta)^2 + (kC_l\delta + \phi)^2]^{1/2}$.

The quantities X_l, C_l and Z_l are given in table 1.

References

[1] H.W. Schnopper, L.P. van Speybroeck, J.P. Delvaille, A. Epstein, E. Källne, R.Z. Bachrach, J.H. Dijkstra and L.J. Lantward, Appl. Opt. 16 (1977) 1088.

[2] E. Källne, H.W. Schnopper, J.P. Delvaille, L.P. van Speybroeck and R.Z. Bachrach, Nucl. Instr. and Meth. 152 (1978) 103.

[3] K.P. Beuermann, R. Lenzen and H. Bräuninger, Appl. Opt. 16 (1977) 1425.

[4] H. Bräuninger, P. Predehl and K.P. Beuermann, Appl. Opt. 18 (1977) 368.

[5] J.H. Dijkstra and L.J. Lantwaard, Opt. Commun. 15 (1975) 300.

[6] F.C. Brown, R.Z. Bachrach and N. Lien, Nucl. Instr. and Meth. 152 (1978) 73.

[7] K. Brunner and W. Hink, Proc. Int. Conf. on X-ray and VUV spectroscopy, Sendai, 1978, Jap. J. Appl. Phys. 17 (1978) suppl. 17-2, 380.

[8] R. Tatchyn, in Workshop of X-ray instrumentation for synchrotron radiation, Stanford, SSRL Report 78/04 (1978) p. VI-67.

[9] H.J. Hagemann, W. Gudat and C. Kunz, J. Opt. Soc. Am. 65 (1975) 742; DESY report SR-74/7.

[10] R. Tatchyn, I. Lindau and E. Källne, these Proceedings, p. 315.

[11] E. Spiller, in Workshop of X-ray instrumentation for synchrotron radiation, Stanford, SSRL Report 78/04 (1978) p. VI-44.